STScI | SPACE TELESCOPE SCIENCE INSTITUTE

Instrument Science Report WFC3 2021-16

WFC3/UVIS: Deuterium Lamp and Filter Performance 2009-2021

Benjamin Kuhn & Harish Khandrika

December 6, 2021

Abstract

We use Wide Field Camera 3/UVIS internal flat-fields taken with the calibration subsystem deuterium lamp between the Servicing Mission Orbital Verification (SMOV) in August 2009 and May 2021 to document changes in the ultraviolet filters and to track the performance of the deuterium lamp. The internal calibration subsystem uses a much different f-ratio (∼f/300) than external science images (f/31) and therefore these flat-fields are not used in the `calwf3` *calibration pipeline to directly correct science exposures. The comparison of the flat-fields taken in December 2020 & May 2021 to those taken during SMOV show a drop of 1-12% in flux (normalized to SMOV) depending on the filter. The drop for the bluest filters (F218W - F280N) is several times higher than for the redder filters implying that the deuterium lamp may be reddening with time. Only ∼2% of the decrease in the ratio images can be accounted for by the UVIS photometric sensitivity losses. One new feature, named the "bowling pin", has been discovered in the flat-fields and the cause remains unknown at this time. The bowling pin is an amorphous region of pixels mostly on the quadrant B side of UVIS1 that shows a decreased signal level compared to the median of the image. The rate of signal decline is increasing over time, and the affected pixel area is also increasing. Additionally, the feature exhibits a color dependence where the affected pixel area and the decrease in signal compared to the median is greatest at shorter wavelengths. The pixels within the bowling pin are ∼1-5% below the median pixel value of the ratio image depending on filter and epoch. All of the previously reported filter and deuterium lamp artifacts remain unchanged: there are no new droplets or dust motes, and the downturn of signal at the outer corner and edge of quadrants B, C, and D is still in agreement with values last recorded by Baggett (2007).*

1 Introduction

One of the routine monitoring programs carried out each cycle on the UVIS detector is the acquisition of internal flat-fields. The WFC3 instrument has four tungsten lamps and one deuterium lamp that are used to stimulate the detector and capture many characteristics, including the presence of prominent new filter features and the performance of the calibration lamps by comparing the flat-fields over time. This program also allows us to track the stability of the pixel-to-pixel sensitivity in all the filters. There is a significant difference between the parameters of an internal flat-field and an external science image. The flat-field lamps are housed in a unique calibration subsystem that produces a highly collimated beam and lowers the usual external science f-ratio from f/31 to ∼f/300 (Baggett, Sabbi, and McCullough 2009). This makes the flat-fields unusable in calibration pipelines, such as `calwf3`[1], to directly correct science observations. One result of using a highly collimated beam (f/300) is that the effects of most features become amplified, and it accentuates artifacts that are not normally seen in science images. The analyses and results presented in this report are therefore used as a means to identify issues with the calibration subsystem itself (e.g. lamp performance and new filter artifacts).

In the past several years, published Instrument Science Reports (ISR) examined the flat-fields for aspects such as pixel-to-pixel variations (Gunning, Baggett, and MacKenty 2014), spatial accuracy (Mack, Rajan, and Bowers 2015), and creating reference files that account for chip dependence (Mack, Dahlen, et al. 2016). The last report to provide a high level performance review of the filters and lamps was Rajan and Baggett (2010), which investigated flat-fields taken during the Servicing Mission Orbital Verification (SMOV) in 2009 shortly after WFC3 installation. In this report we provide a high level assessment of almost 12 years of on-orbit flat-fields taken with the deuterium lamp; for corresponding analysis of tungsten lamp data, see Khandrika and Kuhn (2021). We analyze every flat-field visually and measure the median pixel values over time. To better understand how the filters and deuterium lamp have changed since WFC3 was installed, we normalize to the flat-fields from SMOV as a reference.

2 Data and Analysis Methods

2.1 Data and Calibration

The deuterium lamp flat-field images in this report were taken on-orbit between SMOV (2009 August 17 or 2009.63) and Cycle 28 (2021 May 10 or 2021.35). They are all full-frame images with 1×1 binning and no post-flash or charge injection. Table 1 (in the appendix) lists all of the program IDs, date ranges, and number of images for each of the 14 filters. Twelve of the 14 filters have between 24 and 67 images from 2009.63 - 2020.97, but filters F225W and F336W have 224 and 193 images respectively from 2009.63 - 2021.35.

We retrieved all of the `raw` files from MAST[2] via the Python `astroquery.mast` package.

[1] https://wfc3tools.readthedocs.io/en/latest/wfc3tools/calwf3.html
[2] Mikulski Archive for Space Telescopes - https://mast.stsci.edu/

The files were then calibrated with an over-scan and superbias correction followed by a dark current subtraction using `calwf3 v3.6.0` (`DQICORR, BLEVCORR, BIASCORR,` and `DARKCORR` set to perform). In addition to generating calibrated `flt` files we also made calibrated charge transfer efficiency (CTE) corrected `flc` files. These files were used to verify that any apparent changes in filter or lamp performance were not a product of degrading CTE.

2.2 Analysis Methods

In order to track deviations in the filter and lamp performance throughout UVIS's on-orbit lifetime, we computed filter-by-filter ratios of the individual `flt` images against a reference image created from the flat-fields taken during SMOV (program 11428). The median pixel value of the ratio was saved for both UVIS1 and UVIS2 per filter and analyzed as a function of time. The flat-fields taken during SMOV spanned three days from August 17 - 19, 2009 and represent the first deuterium flat-fields obtained on-orbit after WFC3 was installed. Each filter had four images taken during SMOV that we median combined together to create a single reference image per filter. First, we convert the units of the flat-fields from counts to counts per second because there are at least two exposure times used for a given filter. Analyzing the evolution of the median count-rate of UVIS1 & UVIS2 in the `flt` files (for a given filter) from 2009 to 2021 allowed us to track the lamp brightness.

Along with analyzing the median count-rate values and the median ratio to SMOV as a function of time, we also conducted a careful visual inspection of the flat-fields and ratio images for artifacts. The ratio images were created per filter and include a color bar that correlates color to pixel values. Human verified pattern recognition is a key way to identify new features such as dust motes or droplets and allowed us to characterize any substantial variations in the flat-fields. We visually examined the ratio images of individual exposures and yearly median combined images. The ratios of the individual `flt` exposures help pinpoint the epoch where a new feature may appear and determine if any outlier values are due to the presence of an artifact. The median combined ratio images enabled us to monitor the overall changes to the flat-fields from year to year.

3 Results

3.1 Deuterium Lamp Performance

Figure 1 shows the median ratio to SMOV value for every available on-orbit deuterium flat-field separated by filter type. Performing a linear least-squares fit yields a rate of change between -0.04 and -0.43% per year depending on the filter type. After almost 12 years, those slopes correspond to a drop in the ratio of ∼0.5-5%. Similar to Figure 1, Figure 2 also illustrates the ratio to SMOV for each filter, but here we plot the values as a function of the filter pivot wavelength and only the ratio of the most recent flat-fields to SMOV are shown (December 2020 -May 2021). A majority of the filters experience a drop of ∼1-6%, but the filters with a pivot wavelength shorter than ∼3354 Å (F336W) exhibit a drop of ∼7-12%. Bluer filters experiencing a larger decline could be evidence that the deuterium lamp is reddening over time.

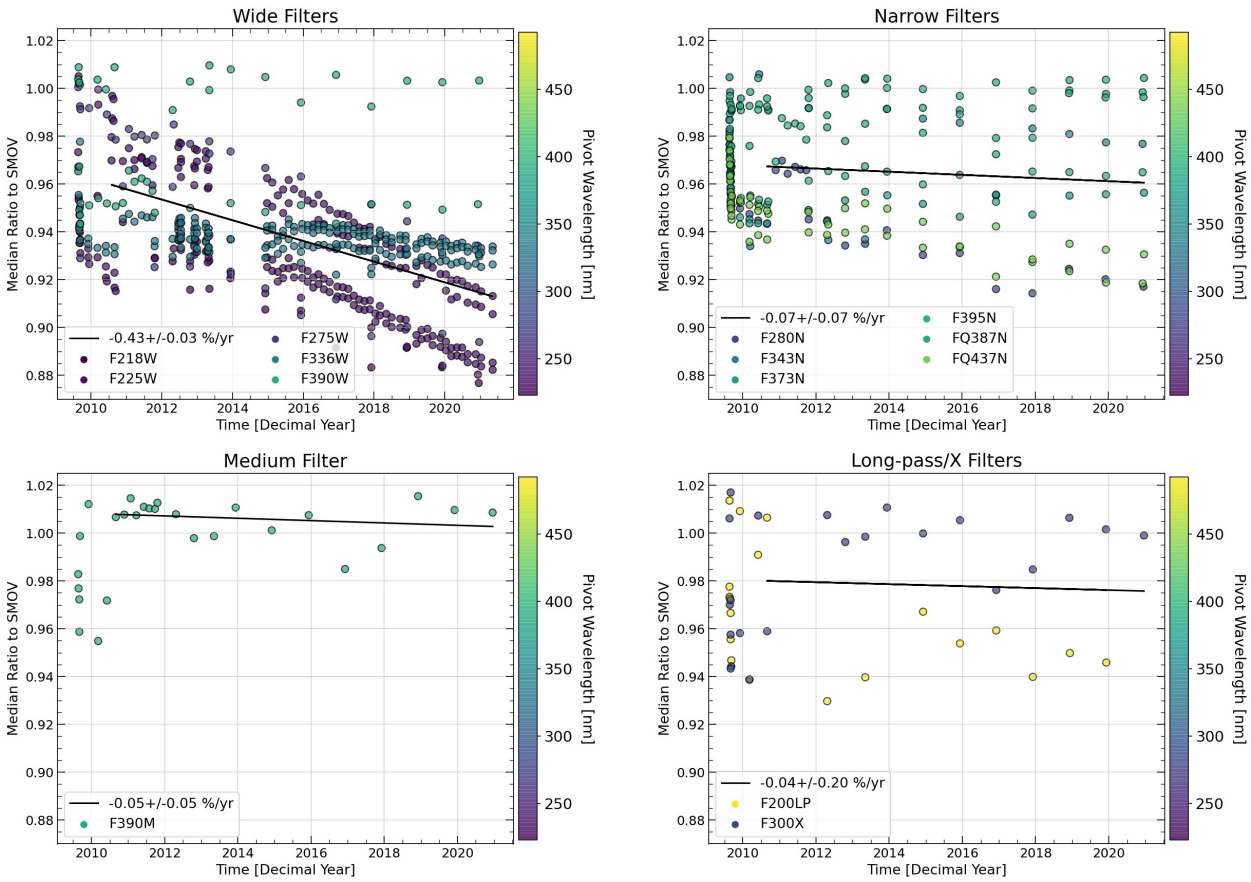

Figure 1: Ratios of the median count-rate of all the flat-fields to the SMOV reference flat separated by filter type and colored by pivot wavelength (in nm). From top to bottom, left to right, the panels in the figure show: the wide filters, narrow filters, medium filter, and the long-pass/extremely wide filters. The black line in each panel is a linear least-squares fit to the data with the slope and standard error presented in the legend.

We were able to verify that the decline in performance was not due to degrading CTE by measuring both `flt` and `flc` files, as shown in Figure 2. With the exception of the quad filters, the ratios from the CTE-corrected flats fall directly on top of those from the `flt` files. In addition to the ratio values, Figure 2 also contains the photometric sensitivity losses reported by Calamida et al. (2021) for UVIS1 and UVIS2 as of 2021. As depicted in the plot, the overall decline in the ratios can only partially be attributed to the photometric sensitivity decline of the UVIS detector, with the majority of the filters across all pivot wavelengths showing larger losses than the sensitivity losses. The exact values plotted in Figure 2 as well as the epoch of observation are listed in Table 2 (in the appendix).

Observers interested in viewing the evolution for each individual filter may visit the UVIS calibration subsystem webpage https://www.stsci.edu/hst/instrumentation/wfc3/performance/cal-subsystem. This page contains all of the internal flat-field and ratio images, separated by filter, using both the deruterium and tungsten lamps. Additionally, plots of the median ratio and count-rate values as a function of time for each filter are hosted on the page.

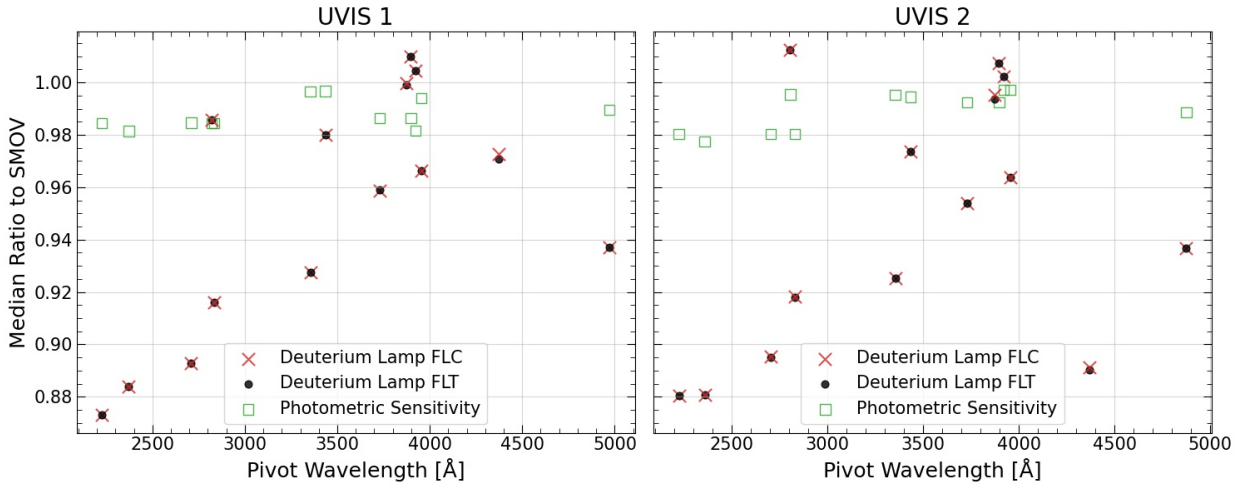

Figure 2: Ratios of the median count-rate of internal deuterium lamp flat-field images versus pivot wavelength (in angstroms) for the most recent exposures (2020.94 - 2021.35). The left panel shows ratios of UVIS 1 and the right panel shows UVIS 2. The red X's represent the ratios using `flc` files and the black circles are for `flt` files. The `flt` and `flc` values fall directly on top of each other. The open green squares are the photometric sensitivity losses as of 2021 reported by Calamida et al. (2021). The exact values being plotted as well as the epoch of the observations are listed in Table 2 in the appendix.

3.2 New Artifact in Deuterium Lamp Flat-Fields: The Bowling Pin

During the visual inspection of the ratio images, a previously unreported feature was found on UVIS1. The feature resides mostly on the Amplifier B (right) side of UVIS1, but a small portion of the feature extends into the Amplifier A side. The feature is defined by pixels with a lower ratio value compared to the rest of the image. The decline of signal and size of the feature have been increasing since 2009, affecting the bluest filters the most, and largely disappearing in filters F390M&W, F395N, FQ387N, and FQ437N. The artifact is also seen in tungsten lamp flat-field ratios, and does not appear by filter F547M (Khandrika and Kuhn 2021). Sampling pixels within the bowling pin for flat-fields taken with the bluest filter, F218W, show a ∼1% drop below the median in 2009 and ∼5% in 2020. In contrast, the drop below the median in the more red F395N filter is only ∼0.1% and 0.2% in 2009 and 2020. Figure 3 shows ratio images of each of the 14 filters from 2020 (2021 for F225W and F336W). The feature was named the "bowling pin" because of the shape seen in the 2020 ratio images. The tight image stretch (±2.5%) in Figure 3 was chosen to accentuate and highlight the bowling pin feature.

In Figure 4 we show two F225W flat-fields, corresponding ratio images and column median plots from September 2009 and May 2021. Both ratio images (Figure 4, middle column) have a white square aperture over-plotted that is 50×50 pixels. We used this aperture to sample some of the pixels that fall within the bowling pin feature. The bowling pin is barely visible in the 2009 ratio image and the average pixel value within the aperture is 0.93, which

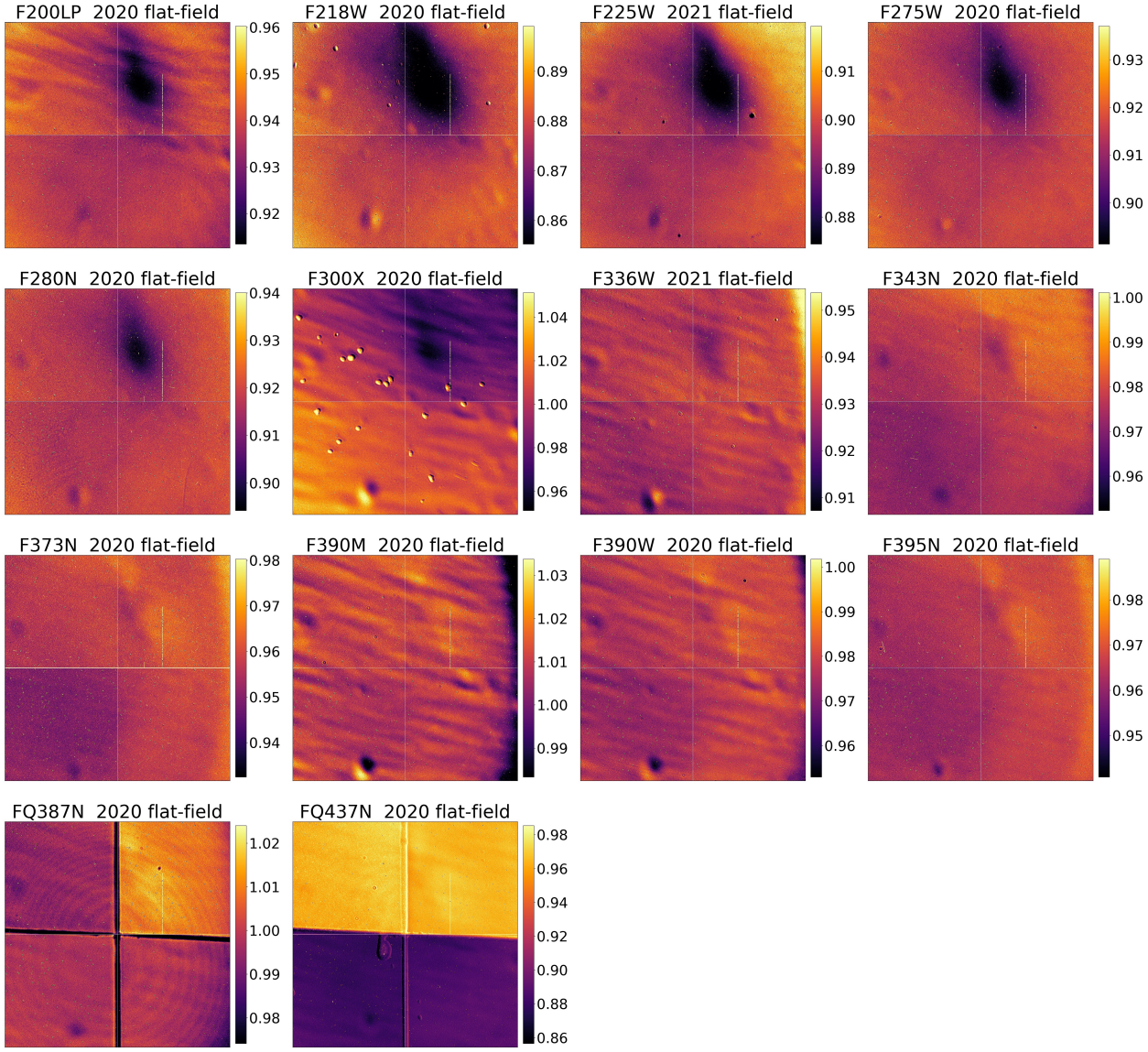

Figure 3: Median combined deuterium lamp flat-fields normalized to SMOV, using all available data from from 2020 (2021 for F225W and F336W). The stretch for F300X (second row, second column) and FQ437N (fourth row, second column) is ±5% and ±7% of the median respectively, while the remaining filters have a stretch of ±2.5% the median. For presentation purposes each image has a thin white line plotted at $x = 2048$ and $y = 2051$ to separate the detector quadrants (A,B,D,C from upper left clockwise to lower left).

is only 1% below the median pixel value of the entire image. In the 2021 ratio image the bowling pin is glaringly visible; with the ±2.5% stretch on the image the feature extends more than 1000 pixels in the y-direction and more than 500 pixels in the x-direction. The average pixel value within the aperture in the 2021 ratio image is 0.85, which is 3% below the median of the whole image. The column median plots on the right side of Figure 4 show the median pixel value of every column in the ratio images with UVIS1 plotted in black and UVIS2 plotted in red. These plots highlight the approximate width and strength of the

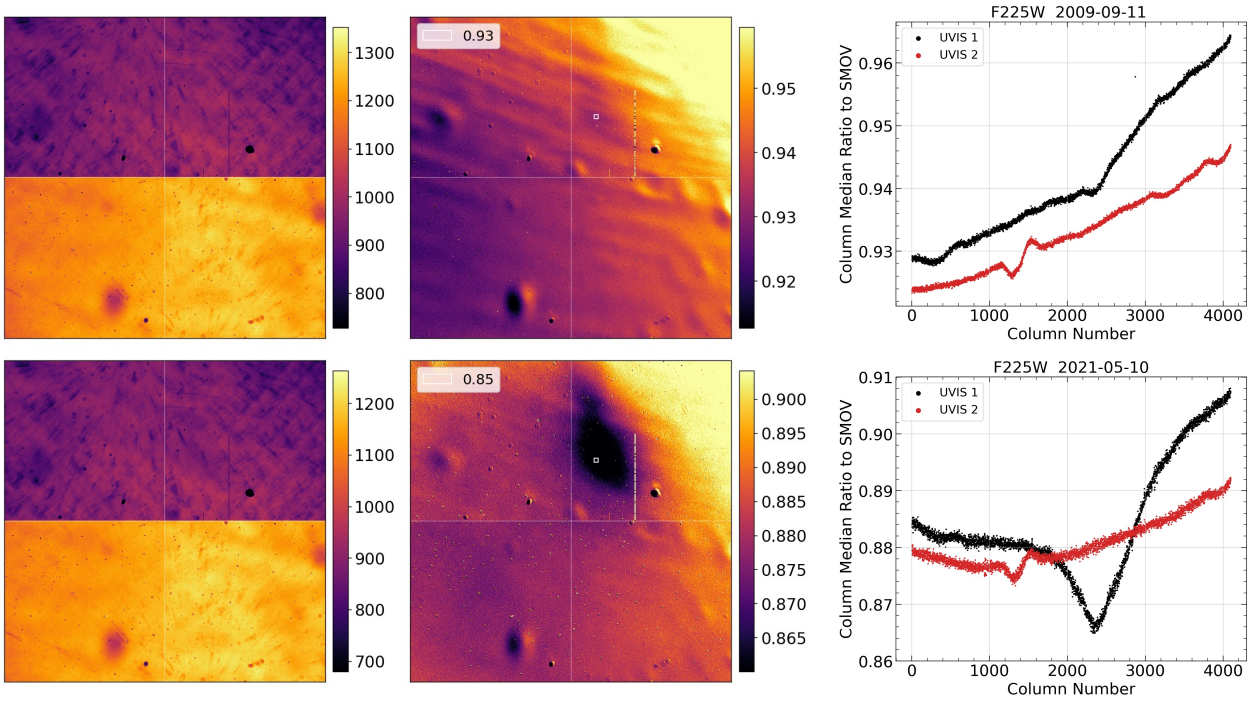

Figure 4: The top row consists of three F225W filter figures from September 2009. The left panel is an internal flat using the deuterium lamp (file `iac50axwq`), in units of counts per second with a stretch of ±30% of the median. The middle panel is a ratio image of the flat-field in the left panel to the SMOV reference flat with a stretch of ±2.5% of the median. The plot on the right shows the median column value (for each column) of the ratio image in the middle panel. UVIS 1 is plotted in black and UVIS 2 in red. The bottom row is the same as the top, but for the F225W flat from May 2021 (file `iegn04diq`). Both ratio images in the middle column have a white square aperture over-plotted that is 50×50 pixels; for those images, the number in the legend corresponds to the average ratio value within the square aperture. In 2009 the average value in the aperture is 0.93 (∼1% below the median) and in 2021 it is 0.85 (∼3% below the median).

bowling pin in the two ratio images.

The cause of the bowling pin is still unknown at this time. We can, however, rule out the possibility that the bowling pin is caused by something on the deuterium lamp housing because the feature is also seen in the tungsten lamp ratio images (Khandrika and Kuhn 2021). Although the bowling pin is in the rough general area of the flat-field 'flare' feature (Mack, Sabbi, and Dahlen 2013), the shape of the flare does not match the bowling pin. Furthermore, the size and strength of the flare have not changed significantly between 2009 and 2020 images, unlike the bowling pin. We evaluated ratios of strongly post-flashed (∼7300 e^-/pixel) dark images separated by ∼9 years. The post-flash LED is located near the UVIS shutter and thus does not travel through the calibration subsystem optics as well as most of the UVIS instrument optics. In the event that the bowling pin was caused by a CCD issue, we would expect the large baseline between the exposures, coupled with the high post-flash, should have emphasized the dark patch (lower value pixels) if it were present. Instead, the

ratio of the dark exposures yielded a mostly flat image with nothing resembling the bowling pin. The results are not definitive, since the bowling pin fades away at visible wavelengths it may be the post-flash images, generated with a very red LED (> 8000 Å), are insensitive to the feature. Further analysis will be required to determine the cause of the bowling pin.

3.3 Known Artifacts in Deuterium Lamp Flat-Fields

All of the UV filters exhibit a crosshatch pattern caused by the laser annealing process during the manufacturing of the CCD (Rajan and Baggett 2010). The artifact is stronger in UVIS1 than UVIS2 and does not appear at wavelengths greater than ∼500 nm. Figure 5 provides an example of what the crosshatch looks like in all 14 filters. The spatial structure of the crosshatch is ∼50-100 pixels and the measured count-rate varies on the order of ∼1-5% depending on filter. In 2016, improved UV flat-fields that correct for the sensitivity residuals of the crosshatch were submitted to the Calibration Reference Data System (Mack 2016).

Another artifact seen in the UVIS flat-fields is called a droplet. These are caused by mineral residue on the outer window of the UVIS detector and show up in a nonuniform distribution across the entire field of view (Brown, Hartig, and Baggett 2008). Figure 6 shows quadrant D (∼2K×2K pixels) of a F225W flat-field from 2021 where the droplets look like a tiny bulls-eye, with a small white point source within a black circle all enclosed by a white ring. They have a diameter of ∼20-30 pixels with a bright saturated core that has a diameter of ∼5-10 pixels. Similar to the droplets, there are also dust motes seen in the UVIS flat-fields as well. Dust motes are pictured in Figure 6 and look like small black spots with diameters similar to the droplets. No new droplets or dust motes have appeared in the internal flat-fields.

As noted by Baggett (2007), there is also a downturn in flux at the outer corners and edges of quadrant B, D and to a smaller degree quadrant C that is attributed to vignetting due to the highly collimated beam (f/300) that is not seen in science images (f/31). These roll-offs at the edge of the flat-fields are worse for the redder filters such as F336W through F395N as well as the quad filters. The vignette can be seen in Figure 5 where we show a median combined flat-field from 2020 (or 2021 when available) of all 14 filters. The decrease in flux has not changed over the years with Amp B, C, and D showing a drop in count-rate of ∼10-40%, ∼5-10%, and ∼10-30% respectively, depending on filter.

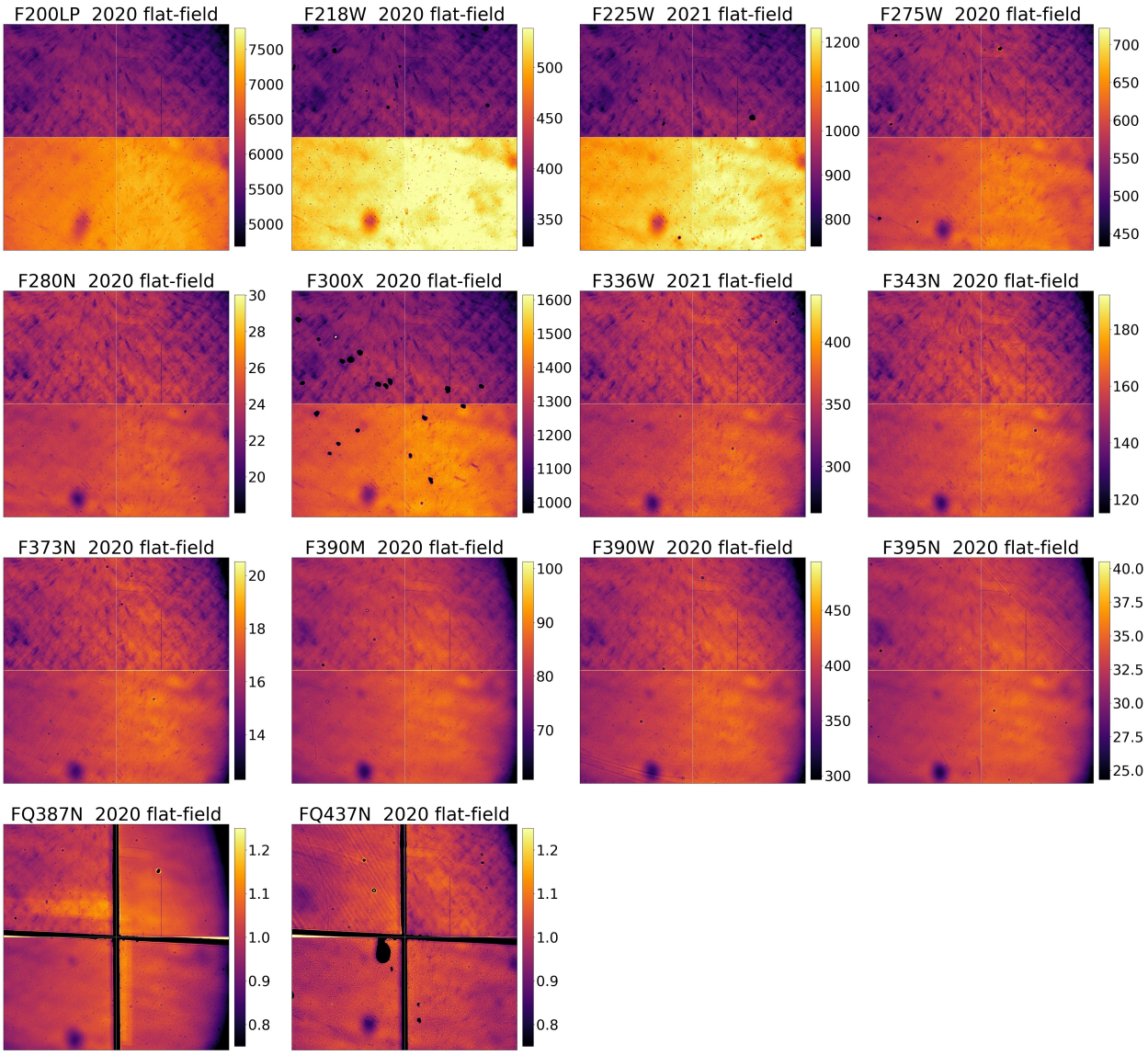

Figure 5: Median combined deuterium lamp flat-fields, in units of counts per second, using all available data from from 2020 (2021 for F225W and F336W). The stretch for F218W and F225W is ±25% of the median. The remaining filters have a stretch of ±15% the median. For the quad filter flat-fields, each quadrant was divided by the median pixel value of the quadrant in order to show all of the features. The color bars for the quad filters are therefore unit-less. For presentation purposes, a thin white line has been added at $x = 2048$ and $y = 2051$ to delineate the detector quadrants.

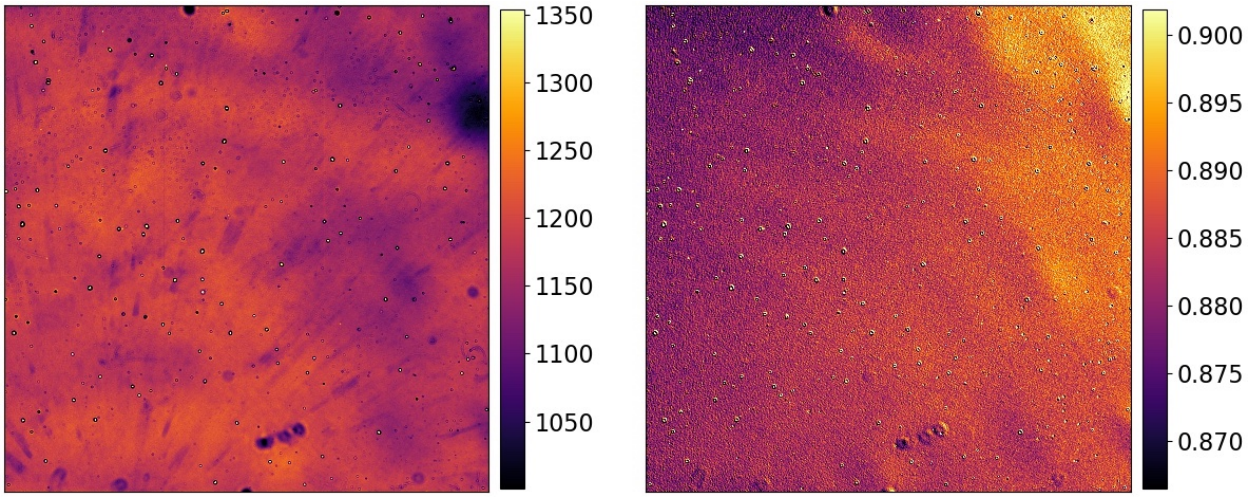

Figure 6: Quadrant D of a F225W internal deuterium lamp flat-field from May 2021 in the left panel and the corresponding ratio to SMOV image in the right panel. The flat-field is in units of counts per second with a stretch of ±15% the median of the quadrant while the ratio image has a stretch of ±2% the median of the quadrant. The small dark spots are dust motes and the spots with bright cores are droplets (mineral deposits). The three dark purple artifacts toward the bottom of the quadrant are features on the filter itself as they are seen in all F225W flat-fields. The large dark spot on the upper right edge of the image section is seen in all filters, but not the tungsten flat-fields, and thus likely caused by something on the deuterium lamp housing.

4 Summary

- Applying a linear least-squares fit to the medians normalized to SMOV levels separated by filter type gives a rate of decline of -0.04 to -0.43% per year (Figure 1).
- After ∼12 years the overall drop in the deuterium lamp median flux levels is ∼1-12%, depending on filter (Figures 1 and 2).
- The bluest filters (F218W - F280N) show the greatest losses, which could be consistent with a reddening of the deuterium lamp. In 2020, the ratio to SMOV for flat-fields in filters F218W, F225W, and F275W showed a total decrease of ∼7-12%. Based on the photometric sensitivity slopes provided by Calamida et al. (2021), we attribute ∼2% of the losses to UVIS sensitivity losses, and count-rate decline is not related to diminishing CTE. (Figure 2)
- A new feature, called the "bowling pin", was discovered in the image ratios relative to SMOV. The artifact is color dependent, affecting the bluest filters the most, and does not seem to appear in filters redder than F373N. The apparent size of the bowling pin has been increasing over time and the values of the pixels, normalized to SMOV, have been decreasing. Tracking flux levels (normalized to SMOV) via a 50x50 pixel aperture

within the bowling pin feature shows that in F225W the bowling pin is ∼1%, and 3% below the median value in 2009 and 2021 respectively (Figures 3 and 4).

- The cause of the bowling pin is unknown and further work will be needed to investigate the cause and characterize the effects.

- All of the previously reported deuterium lamp flat-field artifacts have not changed since they were discovered. The "crosshatch" remains stronger in UVIS1 with the observed count-rate dropping ∼1-5% depending on the filter. The number, size, and strength of the "droplets" and dust motes have stayed the same. And lastly, the downturn in flux at the outer corner and edge of quadrants B, C, and D is still 10-40%, 5-10%, and 10-30% respectively depending on wavelength (Figures 5 and 6).

- We have set up a website to host all of the internal flat-field and ratio images, separated by filter, using both the deuterium and tungsten lamps. We also provide plots of the median ratio and count-rate values as a function of time for each individual filter. https://www.stsci.edu/hst/instrumentation/wfc3/performance/cal-subsystem

Acknowledgements

The authors thank Sylvia Baggett for her review of this ISR and invaluable guidance throughout the project. We are also grateful to Annalisa Calamida, Mariarosa Marinelli, and Joel Green for thoroughly reviewing this ISR and providing many comments and edits that helped strengthen the report.

References

Baggett (May 2007). *WFC3 Ambient-2 Testing: Calibration Subsystem Performance*. Space Telescope WFC Instrument Science Report.

Baggett, E. Sabbi, and P. McCullough (Nov. 2009). *WFC3 SMOV Proposal 11422/11529: UVIS SOFA and Lamp Checks*. Space Telescope WFC Instrument Science Report.

Brown, Thomas M., George Hartig, and Baggett (May 2008). *WFC3 TV3 Testing: UVIS Window Contamination*. Space Telescope WFC Instrument Science Report.

Calamida, Annalisa et al. (Feb. 2021). *New time-dependent WFC3 UVIS inverse sensitivities*. Space Telescope WFC Instrument Science Report.

Gunning, H., Baggett, and J. MacKenty (Sept. 2014). *Pixel-to-Pixel Flat field Changes in WFC3/UVIS*. Space Telescope WFC Instrument Science Report.

Khandrika, Harish and Benjamin Kuhn (Sept. 2021). *WFC3/UVIS Tungsten Lamp and Filter Performance 2009-2021*. Space Telescope WFC Instrument Science Report.

Mack, J. (Mar. 2016). *UVIS 2.0: Ultraviolet Flats*. Space Telescope WFC Instrument Science Report.

Mack, J., T. Dahlen, et al. (Mar. 2016). *UVIS 2.0: Chip-Dependent Flats*. Space Telescope WFC Instrument Science Report.

Mack, J., A. Rajan, and A. Bowers (Dec. 2015). *Spatial Accuracy of the UVIS Flat Fields*. Space Telescope WFC Instrument Science Report.

Mack, J., E. Sabbi, and T. Dahlen (June 2013). *In-flight Corrections to the WFC3 UVIS Flat Fields*. Space Telescope WFC Instrument Science Report.

Rajan, A. and Baggett (Jan. 2010). *WFC3 SMOV Proposal 11432: UVIS Internal Flats*. Space Telescope WFC Instrument Science Report.

Appendix

Data used in this report

Table 1: UVIS Deuterium Lamp Internal Flat-Field Observations

Filter	Program IDs (date range)	# of images
F200LP	11428, 11432, 11912, 12711, 13097, 13586, 14028, 14390, 14547, 14997, 15590, 15730, 16410 **(2009.63 - 2020.97)**	24
F218W	11428, 11432, 11912, 12337, 12711, 13097, 13586, 14028, 14390, 14547, 14997, 15590, 15730, 16410 **(2009.63 - 2020.96)**	31
F225W	11428, 11432, 11904, 11912, 12337, 12711, 12808, 13097, 13169, 13586, 14027, 14028, 14389, 14390, 14546, 14547, 14996, 14997, 15589, 15590, 15729, 15730, 16409, 16410 **(2009.63 - 2021.35)**	224
F275W	11428, 11432, 11912, 12337, 12711, 13097, 13586, 14028, 14390, 14547, 14997, 15590, 15730, 16410 **(2009.63 - 2020.97)**	44
F280N	11428, 11432, 11912, 12337, 12711, 13097, 13586, 14028, 14390, 14547, 14997, 15590, 15730, 16410 **(2009.63 - 2020.96)**	37
F300X	11428, 11432, 11912, 12711, 13097, 13586, 14028, 14390, 14547, 14997, 15590, 15730, 16410 **(2009.63 - 2020.96)**	26
F336W	11428, 11432, 11912, 12337, 12711, 12808, 13097, 13169, 13586, 14027, 14028, 14389, 14390, 14546, 14547, 14996, 14997, 15589, 15590, 15729, 15730, 16409, 16410 **(2009.63 - 2021.35)**	193
F343N	11428, 11432, 11912, 12711, 13097, 13586, 14028, 14390, 14547, 14997, 15590, 15730, 16410 **(2009.63 - 2020.94)**	23
F373N	11428, 11432, 11912, 12711, 13097, 13586, 14028, 14390, 14547, 14997, 15590, 15730, 16410 **(2009.63 - 2020.97)**	36
F390M	11428, 11432, 11912, 12337, 12711, 13097, 13586, 14028, 14390, 14547, 14997, 15590, 15730, 16410 **(2009.63 - 2020.96)**	31
F390W	11428, 11432, 11912, 12337, 12711, 13097, 13586, 14028, 14390, 14547, 14997, 15590, 15730, 16410 **(2009.63 - 2020.97)**	47
F395N	11428, 11432, 11912, 12337, 12711, 13097, 13586, 14028, 14390, 14547, 14997, 15590, 15730, 16410 **(2009.63 - 2020.94)**	30
FQ387N	11428, 11432, 11912, 12711, 13097, 13586, 14028, 14390, 14547, 14997, 15590, 15730, 16410 **(2009.63 - 2020.97)**	67
FQ437N	11428, 11432, 11912, 12711, 13097, 13586, 14028, 14390, 14547, 14997, 15590, 15730, 16410 **(2009.63 - 2020.97)**	55

Data Values for Figure 2

Table 2: Most Recent UVIS Deuterium Lamp Flat-Field Ratio to SMOV

Filter	Average Pivot Wavelength (Å)	Ratio to SMOV UVIS 1	Ratio to SMOV UVIS 2	Epoch (Month. Year)
F200LP	4923.5	0.94	0.94	Dec. 2020
F218W	2225.9	0.87	0.88	Dec. 2020
F225W	2365.2	0.88	0.88	May 2021
F275W	2706.5	0.89	0.90	Dec. 2020
F280N	2831.4	0.92	0.92	Dec. 2020
F300X	2813.2	0.99	1.01	Dec. 2020
F336W	3354.6	0.93	0.93	May 2021
F343N	3435.2	0.98	0.97	Dec. 2020
F373N	3730.2	0.96	0.95	Dec. 2020
F390M	3897.1	1.01	1.01	Dec. 2020
F390W	3922.2	1.00	1.00	Dec. 2020
F395N	3955.2	0.97	0.96	Dec. 2020
FQ387N	3874.0	1.01	1.00	Dec. 2020
FQ437N	4371.0	0.97	0.89	Dec. 2020